Int J Appl Earth Obs Geoinformation 93 (2020) 102206

Contents lists available at ScienceDirect

Int J Appl Earth Obs Geoinformation

journal homepage: www.elsevier.com/locate/jag

Mapping forest windthrows using high spatial resolution multispectral satellite images

Michele Dalponte[a,*,1], Sebastian Marzini[a,b,1], Yady Tatiana Solano-Correa[c,1], Giustino Tonon[b], Loris Vescovo[a], Damiano Gianelle[a]

[a] Dept. of Sustainable Agro-Ecosystems and Bioresources, Research and Innovation Centre Fondazione Edmund Mach, via E. Mach 1, 38010 San Michele all'Adige (TN), Italy
[b] Faculty of Science and Technology, Free University of Bolzano-Bozen, Piazza Università 5, 39100 Bolzano, Italy
[c] Center for Information and Communication Technology, Fondazione Bruno Kessler, Via Sommarive 18, 38123 Trento, Italy

ARTICLE INFO

Keywords:
Windthrows mapping
Change vector analysis
Satellite multispectral data
Sentinel-2
PlanetScope
Change detection
Forests

ABSTRACT

Wind disturbances represent the main source of damage in European forests, affecting them directly (windthrows) or indirectly due to secondary damages (insect outbreaks and forest fires). The assessment of windthrows damages is very important to establish adequate management plans and remote sensing can be very useful for this purpose. Many types of optical remote sensing data are available with different spectral, spatial and temporal resolutions, and many options are possible for data acquisition, i.e. immediately after the event or after a certain time. The objective of this study is to compare the windthrows mapping capabilities of two multispectral satellite constellations (i.e. Sentinel-2 and PlanetScope) characterized by very different spectral, spatial and temporal resolutions, and to evaluate the impact of the acquisition conditions on the mapping results. The analysed area, with an extent of 732 km^2, is located in the Trentino-South Tyrol region (Italy) which was affected by the Vaia storm on the 27th-30th of October 2018, causing serious forest damages. The change vector analysis technique was used to detect the windthrows. For each data source, two pairs of images were considered: 1) pre- and post- event images acquired as close as possible to the event; 2) pre- and post- event images acquired at optimal conditions, i.e. at similar phenological state and similar illumination conditions. The results obtained with the two satellite constellations are very similar despite their different resolutions. Data acquired in optimal conditions allowed having the best detection rate (accuracy above 80 %), while data acquired just after the event showed many limitations. Improved spatial resolution (PlanetScope data) allows for a better delineation of the borders of the windthrow areas and of the detection of smaller windthrow patches.

1. Introduction

Disturbances are essential elements of forest environments, driving the natural processes of regeneration and adaptation. Among the different disturbance events, wind is the most important, being responsible for more than 50 % of the primary damages to the forest ecosystems (Schelhaas, 2008). Wind can act on small patches or at the landscape scale and the severity of the damages depends on different factors, but mainly on the intensity of the event. In Europe extreme winds are mostly linked to winter extra-tropical cyclones that develop over the Atlantic ocean due to temperature gradients between the different latitudes (Mitchell, 2013). Usually, such events are preceded by heavy rainfalls, followed by strong wind guts, which reach a speed higher than 120 km/h. Events with a long recurrence interval are more intense and dangerous than those with a short return period. Generally, windthrows happen when trees experience uprooting or stem breakage, particularly when the wind pressure on the tree is higher than the shear strength of the soil and the root system (Ruel, 1995). Different variables influence these dynamics such as topography, soil conditions (soil water content, depth, soil organic matter, permafrost), stand conditions (vertical and horizontal structures, species composition) and management activities (Albrecht et al., 2012; Jalkanen and Mattila, 2000; Mitchell, 2013; Schelhaas, 2008; Seidl et al., 2014). Windthrows events can have considerable economic effects; trees that experience uprooting or stem breakage have a low timber quality due to the different log damages, while those that resist produce reaction wood, which alters

* Corresponding author.
E-mail address: michele.dalponte@fmach.it (M. Dalponte).
[1] Dalponte, Marzini and Solano-Correa should be considered joint first authors.

https://doi.org/10.1016/j.jag.2020.102206
Received 30 May 2020; Received in revised form 16 July 2020; Accepted 16 July 2020

the structure making the timber less desirable for economical purposes. Economic consequences are more serious when the damaged parts of the tree are the most valuable, such as those below the crown. Moreover, secondary disturbances (saproxylic parasites outbreak or fungal infections) concur at reducing the timber value, amplifying the damages also to stand patches that were not directly subjected by a windthrow. Therefore, it is very important to timely map the windthrow areas with a high level of accuracy as timber and other woody debris should be harvested in reasonable time (normally one/two years after the event) to overcome serious economic loss (Moreau et al., 2003).

The detection and delineation of windthrow areas can be done in different ways. Usually, field surveys and aerial imagery interpretation are carried out as a preliminary assessment, though they present many different limitations related to the techniques and the working environment (Rüetschi et al., 2019; Schwarz et al., 2003). Nowadays, remote sensing represents the main cost-effective tool for windthrows detection and analysis. The efficiency in detecting windthrows using optical remote sensing systems depends on different criteria (Schwarz et al., 2003): i) data availability/temporal resolution: operational analysis and assessments need a continuous provisioning of data, thus remote sensing images acquired with a high temporal frequency are decisive. Moreover, images acquired frequently can help to cope with limitations related to the weather (presence of clouds that occlude the information); ii) spectral resolution: the sensor used should acquire several bands sensitive to vegetation changes across the visible and infrared domains (including also both short-wave infrared and near-infrared wavelengths); and iii) spatial resolution, depending on the landscape homogeneity and on the type of damages that need to be mapped (large scale or small scale).

The temporal and spatial resolutions are very important factors to consider. Since the mapping of damages is required as soon as possible after an event, it is important to access data acquired with a high frequency, so the chance to have a clear sky day during an image acquisition after the event should be maximized: a daily product maximizes the probability to get a good image while a weekly product could create significant delays. Frequently, catastrophic natural events, such as storms, happen in seasons characterized by high precipitation and thus cloudy sky is a major constraint. On the other side, remote sensing images obtained in a period soon after the event could not be the best due to high levels of humidity, woody materials on the ground, debris, and the possible presence of snow.

A trade-off between spatial and spectral resolution exists. Regarding the spatial resolution, medium-resolution sensors (e.g. MODIS) are not very helpful in the analysis of forest cover changes, while High spatial Resolution (HR, e.g. Sentinel-2) and Very High Spatial Resolution (VHR, e.g. GeoEye, Quickbird, Ikonos, PlanetScope) data are able to detect small-scale changes or even damaged single-trees, in relation to the heterogeneity/homogeneity of the landscape (Rich et al., 2010). Nevertheless, the application of VHR images in forestry studies involves high costs for the acquisition of such data (Einzmann et al., 2017; Rich et al., 2010). Regarding the spectral resolution, medium resolution sensors usually acquire information in several spectral bands (at the cost of a lower spatial resolution), whereas HR and VHR sensors usually acquire information in four (blue, green, red, and near infrared - NIR) to ten bands (including some Short Wave Infrared bands - SWIR). Green, red, and NIR bands and their combinations provide information related to vegetation phenology and health status, while SWIR bands can be useful to study vegetation properties related to water content (Ceccato et al., 2002, 2001; Vogelmann, 1990). Thus, HR sensors represent a good trade-off between spatial and spectral resolutions.

The identification of windthrows using remote sensing data is not a new topic and in the literature many studies using different methods and different platforms can be found. Different temporal approaches are adopted: there are studies based on single time data (one image before and one after the event - (Rich et al., 2010)) and others using multi temporal data (several images around the event - (Einzmann et al., 2017; Jonikavičius and Mozgeris, 2013; Rüetschi et al., 2019; Schwarz et al., 2003). Regarding the identification methods, some authors are using supervised classification techniques (Einzmann et al., 2017; Schwarz et al., 2003) while others make use of unsupervised thresholding (Jonikavičius and Mozgeris, 2013; Rich et al., 2010). Considering different platforms, the identification of windthrows is often based on satellite data (Einzmann et al., 2017; Jonikavičius and Mozgeris, 2013), although several studies make use of airborne (Hamdi et al., 2019; Wang and Xu, 2010) or UAV data (Duan et al., 2017; Einzmann et al., 2017).

Studies based on single time data use data acquired after the event and in many cases with specific acquisitions from airborne (Hamdi et al., 2019) and UAV platforms (Duan et al., 2017; Einzmann et al., 2017). Multitemporal studies are mainly carried out with satellite data such as e.g. Landsat ETM + data (Jonikavičius and Mozgeris, 2013; Schwarz et al., 2003; Vorovencii, 2014; Wang and Xu, 2010) or including SAR data (Rüetschi et al., 2019; Schwarz et al., 2003; Tanase et al., 2018). Classification techniques include Support Vector Machines (Baumann et al., 2014; Hamdi et al., 2019), Random Forest (Duan et al., 2017; Einzmann et al., 2017) or Maximum Likelihood (Wang and Xu, 2010). Among the unsupervised studies, the detection of the windthrow areas is done mainly by extracting specific indexes like the windthrow index (Rüetschi et al., 2019) or the disturbance index (Baumann et al., 2014; Haidu et al., 2019). A few studies were based on the identification of fallen tree stems and these studies were all based on VHR images (Chirici et al., 2019; Nyström et al., 2014; Pirotti, 2011).

Analysing the literature of remote sensing data, one possible approach to be considered is the Change Detection (CD) one. It is worth noting that this approach is generally not used for windthrows detection. One of the most well-known CD techniques is the Change Vector Analysis (CVA). The principle of CVA is to describe the change of individual features between two dates as a vector within the features space, which can be described by a magnitude and an angle/direction component. The magnitude component expresses the amount of change while the angle/direction component informs about the type of change. This technique is widely used for many different applications such as fire detection, vegetation monitoring, deforestation detection, wetland change detection, agriculture monitoring, among others (Johnson and Kasischke, 1998; Roemer et al., 2010; Singh and Talwar, 2014), but to the best of our knowledge, very few studies exist that have used such technique for windthrows detection (Wang and Xu, 2010). In particular, (Wang and Xu, 2010) compared four CD algorithms to detect hurricane damages to forests. They concluded that CVA, compared with two other methods (post-classification comparison and univariate image differencing), was providing the best results. The full potential of using CVA for detection of windthrows needs to be fully explored, alongside with the relevance of using images acquired at different spectral, spatial and temporal resolutions.

Accordingly, this study aims at comparing the windthrows mapping capabilities of two multispectral satellite constellations (i.e. Sentinel-2 and PlanetScope) characterized by very different spectral, spatial and temporal resolutions, and to evaluate the impact of the acquisition conditions (i.e. sun illumination and phenological phase of the vegetation) on the mapping results. To reach such goals, we analysed two scenarios: one considering data of pre- and post-event as close as possible in time (as allowed by weather conditions) to the windthrows event, and one scenario considering data of pre- and post-event acquired at optimal conditions (i.e. equal phenological phase and equal illumination conditions).

2. Study area and data set description

2.1. Study area

The study area is located in the North-East of the Autonomous

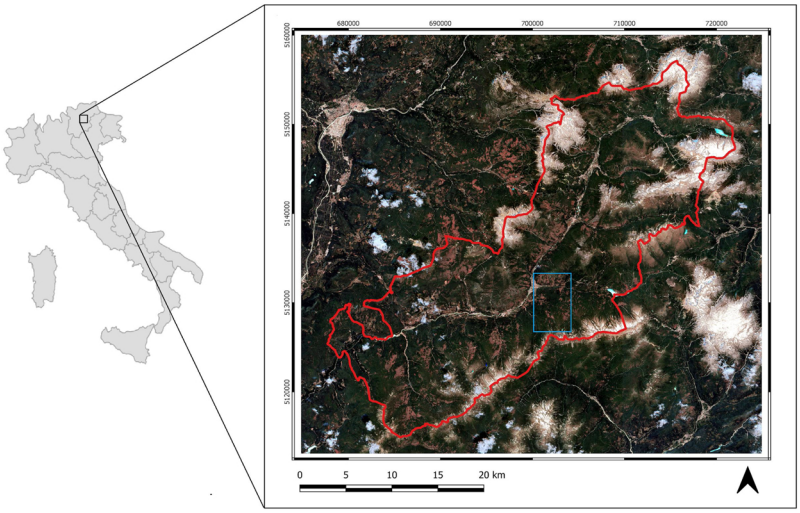

Fig. 1. S2 satellite image (10 m resolution) of the area analysed with the administrative boundaries (red line) of the valleys interested by this study and the subset area used for as manual reference (blue line). (For interpretation of the references to colour in this figure legend, the reader is referred to the web version of this article).

Province of Trento (PAT) in Italy (Fig. 1) and it includes the forest areas of the administrative districts of the Fiemme and Fassa valleys. The total extension of the area is 732 km^2 out of which 454 km^2 are forests. The most common tree species include Norway spruce (*Picea abies* (L.) H. Karst), silver fir (*Abies alba* Mill.) and European beech (*Fagus sylvatica* L.). The landscape is primarily mountainous. The location and the extension of the study area was chosen as it was heavily hit by a windthrows event.

Between the 27th and the 30th of October 2018, the North East of Italy was hit by the Vaia storm, one of the most intense storm events of the country in the last decades. The precipitations during the storm were very severe fluctuating around 300 − 400 mm (Cat Berro et al., 2018): they were more intense on mountain areas (with peaks of 800 mm) including severe snowfalls at higher altitudes. Winds reached peaks of 200 km/h. The consequences were different: in many mountain valleys rivers and streams flooded, triggering debris flows and landslides that impacted both facilities and infrastructures with multiple and several damages and also some casualties. Quantification of forest damages was carried out by local Government entities (Forest Service of PAT) by field surveys and photo-interpretation on satellite images (a windthrows map was produced from this analysis). From this first quantification, inside our study area, a total of 59.4 km^2 of forest were damaged (out of 454 km^2). These quantifications are not really reliable due to the techniques used to quantify the damages right after the event, together with the vegetation and meteorological conditions (e.g. phenology changes, presence of snow, high cloud coverage) related to the interested sites. Field operations (salvage logging) are still ongoing (as May 2020) to harvest the timber in windthrow areas and will require more than three years of work. Moreover, not all the trees can be collected since on many sites the slope is too steep.

2.2. Data set description

In order to achieve the proposed goals of this research, data from two different sensors were considered: Sentinel-2 (S2) and PlanetScope (PS). These two sensors have different characteristics in terms of spatial, spectral and temporal resolution and thus, we expect to see slightly different results from each of them. Associated with the spectral information (see Table 1) there is also the radiometric quality which could be particularly important for PS, since at higher spatial resolutions the radiometric quality is not always guaranteed. In any case, there are already some studies in literature that have proven the radiometric quality of PS to be similar to that of Landsat (Houborg and McCabe, 2018).

Table 1
Spectral bands and spatial resolution for the Sentinel-2 (S2A & S2B)[a] and PlanetScope sensors[b].

	Sentinel-2			PlanetScope		
	Band	Spectral range (nm)	Spatial resolution (m)	Band	Spectral range (nm)	Spatial resolution (m)
Blue	1	432–453	60	1	455–515	3
	2	459–525	10			
Green	3	542–578	10	2	500–590	3
Red	4	649–680	10	3	590–670	3
NIR	5	697–712	20	4	780–860	3
	6	733–748	20			
	7	773–793	20			
	8	780–886	10			
	8A	854–875	20			
SWIR	9	935–955	60			
	10	1358–1389	60			
	11	1568–1659	20			
	12	2115–2290	20			

[a] https://earth.esa.int/web/sentinel/technical-guides/sentinel-2-msi/msi-instrument.
[b] https://earth.esa.int/web/guest/missions/3rd-party-missions/current-missions/planetscope.

2.2.1. Sentinel-2 data

Sentinel-2 is a constellation of two satellites managed by the European Space Agency (ESA) under the Copernicus programme, providing high spatial resolution (HR) optical imaging every 5 days (with its two satellites). S2 images can be freely downloaded and they are widely used for monitoring changes on the Earth's surface (https://scihub.copernicus.eu/). Each S2 multispectral image has a swath width of 290 km and is composed of 13 spectral bands at three different spatial resolutions (see Table 1). For the purposes of this paper, S2 images of the designated study area were downloaded for four different dates (see Table 2). Two dates were selected as close as possible to the event, before and after it, while two other dates were selected -in June 2018 and 2019- before and after the event to obtain optimal acquisition conditions, i.e. optimal sun angle and comparable forest phenological stage for both images (see Table 2 for phenological phases). Due to the weather conditions typical of the autumn season, and of the fact that S2 has a revisit time of about 5 days the closest images without cloud cover covering the entire study area were quite far from the event, compared to PS data.

Table 2
Acquisition dates and phenological phases (Vilhar et al., 2013) of the images used in this study.

	Satellite	Dates	Illumination condition			Phenological phase	
			Sun altitude	Sun azimuth	Shadow length at an object level 25 m	Conifers	Broadleaves
Pre-event	S2	2018 – 06-23	63.65°	144.78°	12.07 m	Flowering	Flowering
		2018 – 09-26	41.24°	163.97°	28.52 m	Flowering and autumn colouring (just for *Larix decidua* Mill.) depending on the altitude	Flowering and autumn colouring depending on the altitude
	PS	2018 – 06-23	59.29°	129.47°	14.85 m	Flowering	Flowering
		2018 – 10-21	30.27°	157.33°	42.83 m	Autumn colouring (just for *Larix decidua* Mill.)	Autumn colouring
		2018 – 10-22	29.94°	157.48°	43.41 m		
		2018 – 10-24	28.67°	155.36°	45.72 m		
Post-event	S2	2018 – 12-15	20.43°	182.28°	67.13 m	Leaf fall (just for *Larix decidua* Mill.)	Leaf fall
		2019 – 06-28	64.10°	147.76°	12.14 m	Flowering	Flowering
	PS	2018 – 11-14	25.33°	175.27°	52.83 m	Leaf fall (just for *Larix decidua* Mill.)	Leaf fall
		2019 – 06-26	60.34°	132.70°	14.24 m	Flowering	Flowering

2.2.2. PlanetScope data

PlanetScope is a constellation of more than 120 nano-satellites (Dove satellites) owned by the imaging company Planet Labs, Inc. (PlanetTeam, 2017) providing daily HR multispectral images, composed by four spectral bands (see Table 1) at 3 m spatial resolution. Though PS is a commercial satellite, many of its products are open access for research purposes and they can be downloaded from their website (www.planet.com). Each PS multispectral image covers an area of 24 × 8 km. As per the S2 case, images of the designated study area were downloaded for four different dates (see Table 2). In this case, the pre-near event images (22nd of October 2018) were not completely covering the study area (they covered 95.7 % of it) and thus they were mosaicked with images acquired on the 21st (2.8 % of the area) and 24th of October 2018 (1.4 % of the area).

2.3. Ancillary data

Three ancillary data were used for the analyses. All the maps were available as vectorial files and were converted to raster ones (at the corresponding spatial resolution of S2 or PS) for validation analysis.

1 A forest type map of the study area. This map indicates the type of forest present in each cadastral parcel of the study area that is classified as forest. These data are the results of forest management plans based on field inspections. This map was used in order to mask the satellite images and focus only on forest areas.
2 Ground truth PAT map: a map of the windthrows due to the Vaia storm (covering the whole study area) created by the Forest Service of the PAT after the Vaia storm by photo interpretation on two SPOT images acquired the 17th and 27th November 2018 (further details can be found in: (Servizio Foreste e Fauna - Provincia Autonoma di Trento, 2020, 2018)). The initial map was then validated in the field during the clearings of the forest and only 34 % of the photo interpreted areas resulted to be reliable. The map was then updated and 43 % of the original polygons were redefined according to the field surveys, while 23 % were considered unreliable but kept in any case in the map as they were referring to areas complex to reach where scattered windthrows happened. In particular, areas characterized by scattered windthrows were considered as all damaged even if only a part of the trees really felt down. The map used in this study was the most updated one, but due to all these problems it was used only to qualitatively evaluate the CD results obtained with CVA over the entire area.
3 Manual reference map: detailed reference windthrows map delineated by photo interpretation (due to the lack of accuracy of ground truth PAT map). This map was created by the authors over a smaller portion w.r.t. the study area (6.6 km x 4.2 km; 29 km^2; corresponding to the 6% of the forested areas of the study area). This map was built in order to validate the results of the CVA and also to have a reference point with respect to the ground truth PAT map, due to the lack of reliability of the latter one. The area on which it was built is smaller than the study area because of the complexity arising on its construction. VHR images of "Bing maps" (in QGIS software with a spatial resolution of 40 cm (QGIS Development Team, 2020)) available after the event and false colour multitemporal compositions of PS before and after the event (near event images) were used to create this map. The VHR images in QGIS are available in true colour composition (RGB), allowing to easily detect the fallen trees where no shadow occlusions were present. Whereas, the false colour composition of the PS images used was: red band at time 1, green band at time 1, blue band at time 2. Such combination highlights in bright green or magenta colours the pixels where changes have happened, and shows in true colour the areas where no changes have occurred. Comparing the highlighted areas to the ones seen in QGIS, a detailed windthrows map could be built. The size of the manually delineated windthrows areas is ranging from a minimum of 9 m^2 to a maximum of 389,781 m^2 with median value of 288 m^2 and mean value of 3996 m^2.

3. Methods

Fig. 2 presents the general block scheme of the procedure followed in order to map the forest windthrows. Four experiments (see Table 3) were considered to guarantee the detection of windthrows together with two HR optical images, X_1 and X_2, acquired over the affected area at different times, before (t_1) and after (t_2) the event. X_1 and X_2 were first pre-processed to make them homogeneous. They were then used in a CD strategy in order to map the forest windthrows.

3.1. Remote sensing data pre-processing

Both S2 and PS images were retrieved from the corresponding archives already corrected from the geometric and topographic/orthographic point of view. For the atmospheric corrections, PS images were already provided at level 3B (which is atmospherically corrected), whereas S2 images could be found in both L1C (radiance values only) and L2A levels. Nevertheless S2 images close in time to the event were not already available at L2A level. In order to avoid different processing steps from our side and that made by ESA, we decided to download all the S2 images at L1C level and apply atmospheric corrections with

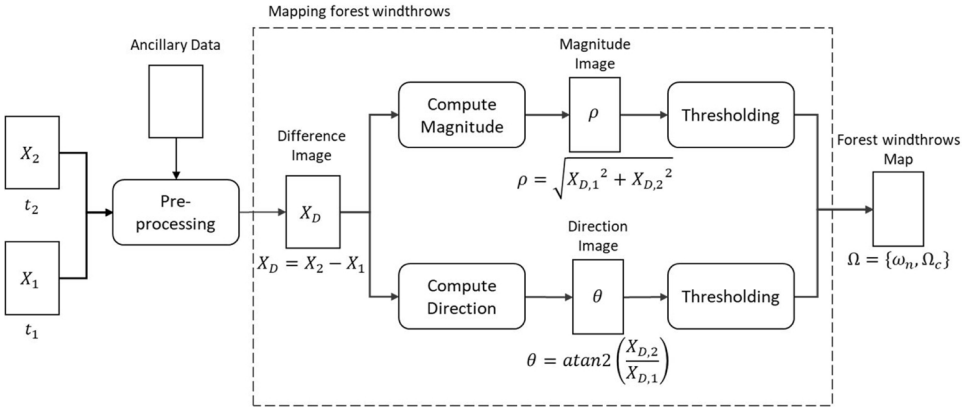

Fig. 2. General block scheme representing the different steps to map forest windthrows.

Table 3
Experiments carried out in this study.

Experiment	Date 1 (X_1)	Date 2 (X_2)	Description
A	June 2018	June 2019	CVA applied to two bands of S2 using data acquired in the same season
B	June 2018	June 2019	CVA applied to two bands of PS using data acquired in the same season
C	September 2018	December 2018	CVA applied to two bands of S2 using data acquired near the event
D	October 2018	November 2018	CVA applied to two bands of PS using data acquired near the event

Sen2Cor[2] by ourselves.

Despite the atmospheric corrections, PS images belonging to different acquisition paths and different days have slightly different reflectance values and thus a relative radiometric normalization (RRN) was carried out in order to get a mosaic to be used for the CVA. In the literature we can find many RRN algorithms (Solano-Correa et al., 2019a; Yong et al., 2001; Yuan and Elvidge, 1996). In order to apply any normalization process, an overlap between the slave (image to be normalized) and the reference image should exist. In our case, overlap along different PS swaths exist. In this study we applied a linear RRN as follows:

$$x_{new} = x * \left(\frac{s_1}{s_2}\right) + \left[m_1 - \left(\frac{s_1}{s_2} * m_2\right)\right] \quad (1)$$

where s_1 and m_1 are the standard deviation and the mean value of the pixels of the reference image in the overlapping part between the two images, s_2 and m_2 are the standard deviation and mean value of the pixels of the of the slave image in the overlapping part between the two images, x is the pixel to be radiometrically normalized, and x_{new} is the relative radiometrically normalized value. This procedure was applied to all the PS mosaics and it allowed us to completely remove all the spectral differences among the images mosaicked.

In order to apply the CVA algorithm, X_1 and X_2 were normalized between 0 and 1, since normalization has been observed to reduce the commission error and to maximize the detection of small-magnitude changes (Johnson and Kasischke, 1998). Moreover all the data were clipped using the map of the forested area in order to analyse only the forested areas and not changes occurred on other land cover types. In the case of S2, all bands at 20 m were re-scaled to 10 m spatial resolution by means of a bilinear interpolation (using the software R, in particular the *resample* function of the package *raster*), and only after all the atmospheric and normalization steps were applied. S2 bands at 60 m were not considered for further analysis, since they were used only for atmospheric correction purposes.

[2] https://step.esa.int/main/third-party-plugins-2/sen2cor/

3.2. Mapping forest windthrows using the CVA technique

The mapping of any disturbance or event in a given study area is nothing else than the detection of the changes happening between two periods of time. To detect such changes, several techniques have been introduced in the literature (Bovolo et al., 2018). Among them, the CVA has been frequently used and explored (though seldom times for windthrows mapping). CVA is an unsupervised technique that does not require reference data in order to detect the changes, though it is limited by the need to select a threshold to separate between changes and no changes. The selection of this threshold can be done in an unsupervised or supervised way (Solano-Correa et al., 2014; Zanetti et al., 2015). CVA exploits both multispectral and multitemporal information by means of the difference operator. The multispectral difference image $X_D = X_2 - X_1$ is composed of spectral change vectors (SCV - $X_{D,1}, \ldots, X_{D,n}$ according to the number of features used). The reason for using the difference operator is that unchanged pixels/areas in an image will show similar (if not equal) spectral responses resulting in SCVs equal or close to zero, whereas changed pixels/areas will show SCVs higher than zero. However, in order to obtain such a result, CVA requires basic pre-processing operations of the raw data that guarantees homogeneous data in terms of both spatial and spectral information.

CVA can work in a *n*-dimensions space, but is mostly used in a two dimension one where information redundancy from different features is reduced. The space dimension is defined by the number of features used to highlight particular types of changes, going from one single feature (when it is better known as univariate image difference) to as many as spectral bands a sensor may have (and possible combinations of those spectral bands). In this study we decided to use a two dimensions space, mainly for two reasons: i) we want to detect just one type of change that is the one caused by windthrows, while we are not interested in other changes; ii) the idea is to have simple system that can be used in practical applications and thus a 2-dimension system appeared to be the best trade-off between complexity and usability. The type of change that we are focusing on is vegetation related, and it is well-known in literature that bands corresponding to the visible and infrared spectrum help to highlight vegetation (Vogelmann, 1990; Xue and Su, 2017). Some examples of such combinations are the Normalized Difference Vegetation Index (red and NIR) and Normalized Difference Water index

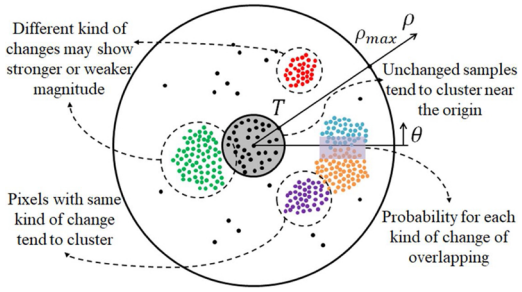

Fig. 3. Representation of CVA in a polar space (modified from (Solano-Correa et al., 2019b)).

(blue and SWIR). In order to render the paper more general, all possible combinations of two bands for both S2 and PS were evaluated, and the best of them (in terms of windthrows detection accuracy) was selected for the analysis.

To effectively map windthrows, X_D vector is represented in polar coordinates by computing the magnitude (ρ) and angle (θ):

$$\rho = \sqrt{X_{D,1}{}^2 + X_{D,2}{}^2} \tag{2}$$

$$\theta = atan2\left(\frac{X_{D,2}}{X_{D,1}}\right) \tag{3}$$

Fig. 3 shows a 2D-CVA exemplary representation, where the main characteristics of the changed and unchanged samples in a polar domain (magnitude and angle) are displayed: i) un-changed samples tend to cluster near the origin (light grey circle); ii) pixels with the same kind of change tend to cluster (coloured clusters); iii) different kind of changes may show stronger or weaker magnitude (green vs red cluster); and iv) there exists a probability for each kind of change of overlapping (orange and blue clusters) (Solano-Correa et al., 2019b, 2016).

According to the previous observations, a magnitude-direction domain (D) can be defined as:

$$D = \{\rho \in [0, \rho_{max}], \theta \in [0,2\pi)\} \tag{4}$$

where ρ_{max} is the maximum magnitude of X_D. A set of thresholds can be applied to both magnitude (T_ρ) and direction (T_θ) variables that allow to separate among changes (Ω_c) and no-changes (ω_n). T_ρ and T_θ can be calculated manually or automatically and they are generally guided by the complexity of the studied problem (Solano-Correa et al., 2014; Zanetti et al., 2015). For the case of this manuscript, we want to be able to map only windthrows, therefore, these thresholds could be calculated in a manual way, but, in order to keep a generalized comparison between S2 and PS, a semi-automatic strategy was implemented. We defined the thresholds testing different combinations of values (in an automatic way) for both the magnitude and angle on the basis of the histogram distribution over a training set and validating the results over a test set. In particular, we set two thresholds for the magnitude ($T_{\rho 1}$, $T_{\rho 2}$) and two thresholds for the angle ($T_{\theta 1}$, $T_{\theta 2}$). We started by taking the windthrows reference map and overlapping a grid of 500m × 500m squares on it. We then split all the squares in two sets, training and test, by selecting each of them in an alternate manner (like a chessboard). For each set, we calculated the CVA and selected the thresholds values based on histogram quantiles of magnitude and direction variables of the training set. In total we considered four thresholds: a minimum and maximum limit for the magnitude and a minimum and maximum limit for the angle. Many combinations of thresholds were tested and the ones providing the highest kappa accuracy and the lowest false and missed alarms on the test set were selected as the optimal one.

3.3. Experimental setup and accuracy assessment

In order to reach the objectives of this study, four experiments were carried out (Table 3). The results of each experiment were assessed defining confusion matrices with respect to the manual reference map in a subset study area where windthrows were carefully delineated by using photo-interpretation. All the confusion matrices were generated considering all the forest areas (initial experiments) and considering only the forest parcels classified by the forest management as Norway spruce and silver fir (additional experiments). These additional experiments helped us to further understand the impact of the time lag (about 11 weeks in the case of S2 images, and about 3 weeks in the case of PS) between the images acquired right before and right after the event. As shown in Table 2 a slight change of vegetation phenology is expected, as in autumn the forest canopy and the understory are undergoing rapid structural and pigment changes. Also, the illumination conditions changed in the time lag considered (Table 2). Conversely, the impact of using images acquired at around the same date (in this case the sun angle is constant, while some inter-annual phenology changes may occur) was also analysed.

In order to avoid redundancy of data, only two bands were selected for the CVA analysis. The selection was carried out by evaluating all possible combinations in the manual reference map area and selecting the two bands providing the best kappa and user accuracy. The best result among the four experiments on the subset area was extended to the entire study area and compared with the ground truth PAT map over the entire study area. Additionally, the reference map and the ground truth PAT map were compared over the subset area in order to see the agreement level among them and in order to validate the ground truth PAT map. All these analyses were carried out using the R software (R Core Team, 2017).

4. Results

Fig. 4 presents the kappa accuracies for different band pairs combinations in the four experiments. It can be clearly seen how the accuracy varies a lot between experiments A–B and C–D. Analyzing experiments A–D we can see that for both S2 and PS the infrared bands play an important role. In particular in experiment A it is clear that in order to obtain good results it is necessary either to combine a band in the visible/red edge part of the spectrum (bands 2, 3, 4, and 5) with one in the NIR (bands 6, 7, 8, and 8A), or one in the NIR (bands 6, 7, 8, and 8A) with one in the SWIR (bands 11 and 12). In experiment B the available bands were less but the trend is very similar. In order to get an accurate detection it is important to combine the NIR band (band 4) with one of the other three. Looking only at the visible part of the spectrum green and red bands (3 and 4 in S2 and 2 and 3 in PS) could also provide good results. In contrast, the kappa accuracies obtained in experiments C and D are not very high, and in none of the cases the kappa value is above 0.25. In any case the trends are quite similar to experiments A and B. The combination of the best bands selected along with the thresholds on the magnitude and angle of the CVA are shown in Table 4. The CVA images were thresholded according to the semi-automatic thresholding done in the bands optimization. Looking at Table 4 it is clear that the thresholds on the angle are constant in the different experiments, while there is a higher variability for the magnitude thresholds even if the ranges are all overlapping. This behaviour is expected given the characteristics of CVA in the polar domain.

In Fig. 5 the windthrow maps generated for the four experiments in the subset area are shown along with the manual reference map and the ground truth PAT map. As it can be visually seen, experiment A, and B have a high level of agreement with the two reference maps, while experiments C and D do not. Among these last two maps it is worth noting how the map obtained in experiment C is less noisy than the one in experiment D and it is possible to see that the main areas present in the reference map are detected but many other additional changes are also detected. Moreover, it can be seen that the reference map and the ground truth PAT map disagree in several areas. We analysed in more details some of the disagreement areas by directly looking at the true

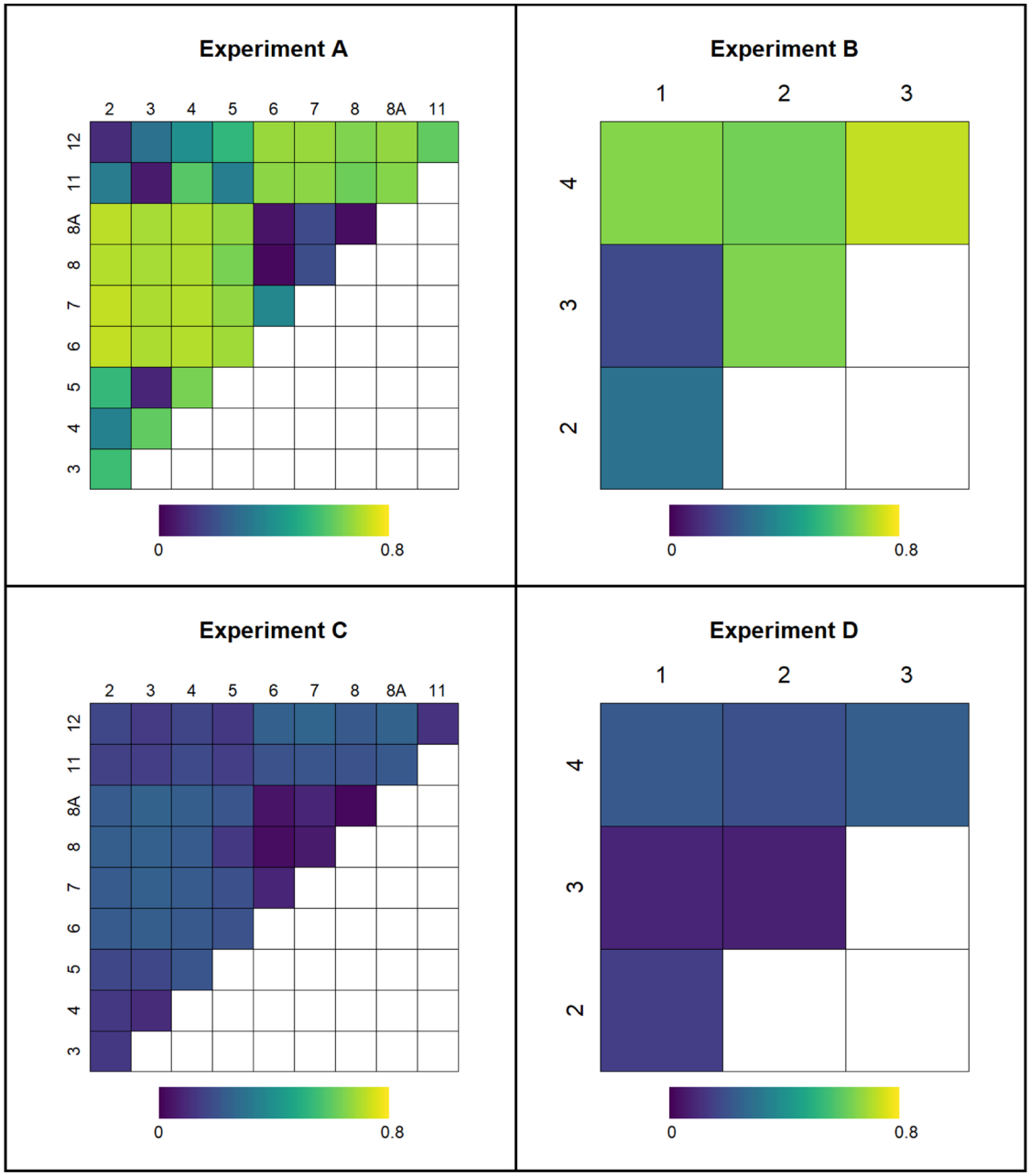

Fig. 4. Kappa accuracies on the test set areas for all the possible pairs of bands combinations in the four experiments.

Table 4
Bands and thresholds T_ρ and T_θ for experiments. A—D.

Experiment	Bands	T_ρ	T_θ
A	2–6	$0.09 < T_\rho < 0.42$	$314 < T_\theta < 316$
B	3–4	$0.16 < T_\rho < 0.80$	$314 < T_\theta < 316$
C	3–8	$0.01 < T_\rho < 0.43$	$314 < T_\theta < 316$
D	1–2	$0.09 < T_\rho < 0.55$	$314 < T_\theta < 316$

colour RGB composition images after the event, and noticed that most of the places marked by the ground truth PAT map as windthrows were actually false alarms corresponding to big areas covered by shadows due to mountains, but clearly not affected by the event, since many big trees were present in the area. The rest of the disagreement corresponds to missed alarms from the ground truth PAT, for small windthrows or improper delineation of existing ones.

Given the results presented in Fig. 5, we performed a comparison among the reference map and the ground truth PAT map in order to understand the level of agreement among them. Table 5 shows the confusion matrix for the ground truth PAT map (delineated by the forest service just after the storm) with respect to the manual reference map over the restricted area. The OA is around 85.9 % (that can be translated as the level of agreement) but the false alarms (225.5 ha), and missed alarms (111.4 ha) are very high. This shows how difficult it is to map the windthrows in a quick way in the field and through photo interpretation just after an event.

Table 6 shows the confusion matrix for the subset area in the four experiments, and it appears clear that experiments A, and B outperformed experiments C and D. Looking at the first two experiments (A and B) we can see that the results are really similar with slightly higher OA and KA in experiment B. In general, the amount of false alarms is higher than the missed alarms. Looking at experiments C and D we can see that experiment C is giving slightly better results than experiment D.

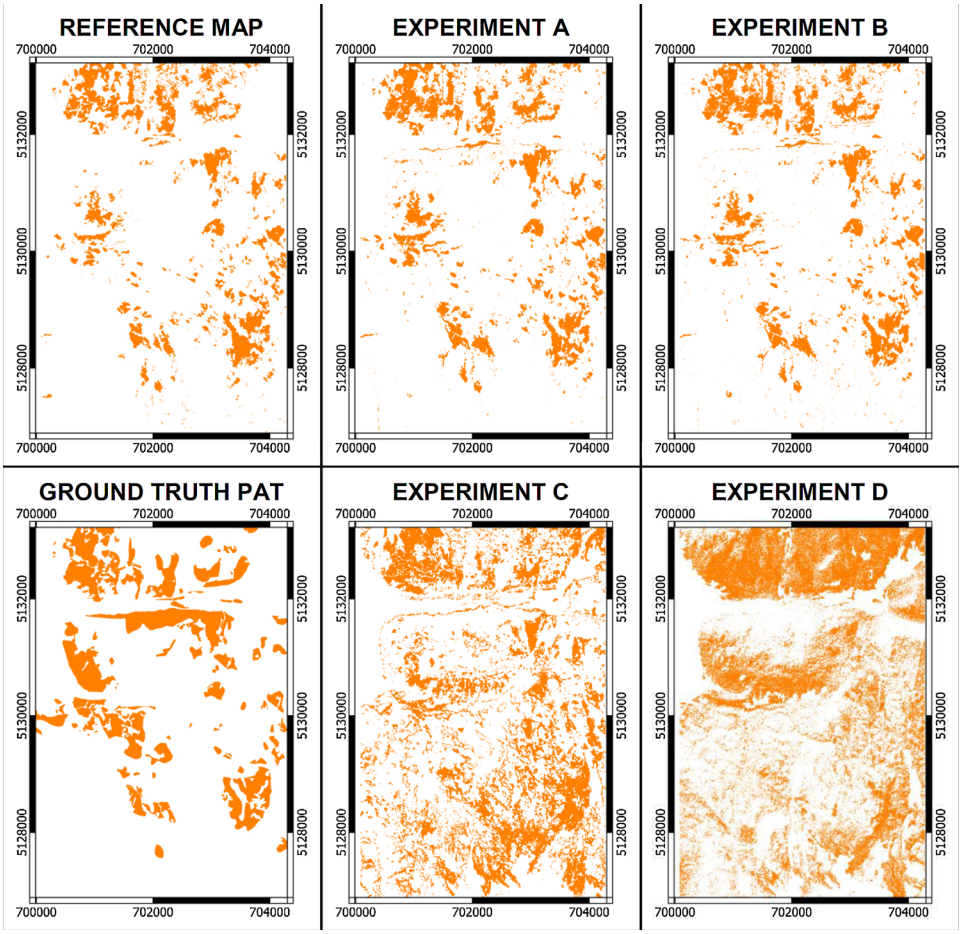

Fig. 5. Windthrows maps for the four experiments in the area in which the reference map was drawn. The manual reference map and the ground truth PAT map are also shown.

Table 5
Confusion matrix for the ground truth PAT map just after the storm with respect to the manual reference map over a restricted area. The numbers are in hectares.

		Manual reference map		User's accuracy (%)
		No windthrow	Windthrow	
Ground truth PAT	No windthrow	1854.7	111.4	94.3
	Windthrow	225.5	196.9	46.6
Producer's accuracy (%)		89.2	63.9	
Overall Accuracy (%)		85.9		
Kappa Accuracy		0.46		

These two experiments had almost identical detection rates for the windthrow class (about 190 ha and PA of about 61 %), very similar missed alarms (about 118 ha and about UA of 92 % for the non-windthrow class) but they have very different false alarms (514.4 ha vs. 666.8 ha). In general, the results in experiments C and D are very poor.

A similar situation can be seen in Table 7, where only areas classified as forests of Norway spruce and silver fir are considered. In this case, it is interesting to note that while the changes in accuracy are very small for experiments A and B, for experiments C and D the false alarms decrease by more than 100 ha.

Fig. 6 shows the density distribution of the aspect for the four experiments in the area where the manual reference map was drown considering the entire area, the correctly detected areas, and the areas of missed and false alarms. As it can be seen while the correctly detected areas have a distribution similar to the one of the entire area, the missed and false alarms are mainly located in a range of aspect around 180 degrees (especially in experiments A and B). This is probably due to the fact that in June on North facing slopes the illumination is more uniform compared to south facing slopes where there are more shadows created by the trees. Moreover, the vast majority of missed and false alarms are located on the borders of the windthrows areas.

From Tables 6 and 7 we selected the best result (experiment B) and we compared the windthrow map obtained in this experiment over the entire study area with the ground truth PAT map (Table 8). These results confirm that there is a big difference between the windthrows

Table 6
Confusion matrices for the four experiments with respect to the manual reference map over a restricted area. The numbers are in hectares. NW = no windthrows; W = windthrows; PA = producer's accuracy; UA = user's accuracy; OA = overall accuracy; KA = kappa accuracy.

A	NW	W	UA (%)	B	NW	W	UA (%)
NW	1992.3	59.4	97.1	NW	1989.9	53.0	97.4
W	88.5	248.9	73.8	W	90.9	255.3	73.7
PA (%)	95.7	80.7		PA (%)	95.6	82.8	
OA (%)	93.8			OA (%)	94.0		
KA	0.74			KA	0.75		

C	NW	W	UA (%)	D	NW	W	UA (%)
NW	1566.3	119.2	92.9	NW	1413.9	117.4	92.3
W	514.4	189.1	26.9	W	666.8	190.9	22.3
PA (%)	75.3	61.3		PA (%)	68.0	61.9	
OA (%)	73.5			OA (%)	67.2		
KA	0.24			KA	0.17		

Table 7
Confusion matrices for the four experiments with respect to the manual reference map over a restricted area considering only parcels of Norway spruce and silver fir. The numbers are in hectares. NW = no windthrows; W = windthrows; PA = producer's accuracy; UA = user's accuracy; OA = overall accuracy; KA = kappa accuracy.

A	NW	W	UA (%)	B	NW	W	UA (%)
NW	1830.4	57.8	96.9	NW	1830.6	51.7	97.3
W	85.1	248.5	74.5	W	84.9	254.6	75.0
PA (%)	95.6	81.1		PA (%)	95.6	83.1	
OA (%)	93.6			OA (%)	93.9		
KA	0.74			KA	0.75		

C	NW	W	UA (%)	D	NW	W	UA (%)
NW	1505.9	118.3	92.7	NW	1341.2	116.3	92.0
W	409.7	187.9	31.4	W	574.3	189.9	24.8
PA (%)	78.6	61.4		PA (%)	70.0	62.0	
OA (%)	76.2			OA (%)	68.9		
KA	0.29			KA	0.20		

maps obtained by photo interpretation, in the weeks just after an event, and those obtained by using remote sensing data and CVA. Moreover, it is worth noting how the results in Table 8 are quite similar to the ones in Table 5 confirming the good agreement between the map in experiment B and the manual reference map.

In Fig. 7 the maps obtained in experiment B, the ground truth PAT map and the difference map among them are shown. From the difference map it is clear that the main difference among the two maps are the areas marked as windthrow in the ground truth PAT map and not detected in experiment B. Analysing in detail such areas, we noticed that they are either areas in steep slope (where in the SPOT image of November 2018 there were shadows), or areas characterized by scattered windthrows. As stated in the report provided by the forest service (Servizio Foreste e Fauna - Provincia Autonoma di Trento, 2020), such areas were kept inside the map even if it was known that the windthrow area amount was over predicted (Servizio Foreste e Fauna - Provincia Autonoma di Trento, 2020). It is interesting to note the red line along Val Cadino (bottom left of Fig. 6) where we detected the change of the vegetation along the river due to the flood connected with the storm,

Table 8
Confusion matrices for the best experiment on the subset area with respect to the ground truth PAT map over the entire area. The numbers are in hectares. NW = no windthrows; W = windthrows; PA = producer's accuracy; UA = user's accuracy; OA = overall accuracy; KA = kappa accuracy.

	NW	W	UA (%)
NW	36952.4	2203.8	94.4
W	3200.2	2883.5	47.4
PA (%)	92.0	56.7	
OA (%)	88.1		
KA	0.45		

while it was not considered in the ground truth PAT map probably as that vegetation is not productive forest.

5. Discussion

In this study we showed that forest windthrows can be mapped with S2 and PS data using CVA, a simple and straightforward CD technique, with high level of accuracy. The analyses that we performed represents a novelty as, at the best of our knowledge, this is the first study that: (i) analyses the use of S2 and PS data to map windthrows; (ii) compares data acquired both near and far from the event; and (iii) analyses the use of CVA to map windthrows.

The two data considered are characterized by very different spectral, spatial, and temporal resolutions. Regarding the spectral resolution, from the band optimization experiment (Fig. 4) it is clear that a band in the NIR is very important. Considering S2, also the SWIR bands (bands 11 and 12) resulted to be useful. These bands are strongly related to leaf water content (Ceccato et al., 2002). The good performance of CVA when the SWIR bands are used may be related to the fact that, after the windthrow, the Norway spruce and silver fir leaf water content - during the time lag between the tree fall and the image acquisition after the event - is varying very quickly, while the pigments remain more constant (Thiagarajan et al., 2016).

The spatial resolution seems to not affect the results as the detection accuracies of S2 and PS obtained in similar conditions (same bands and same dates) are not very different. The main advantage of a higher

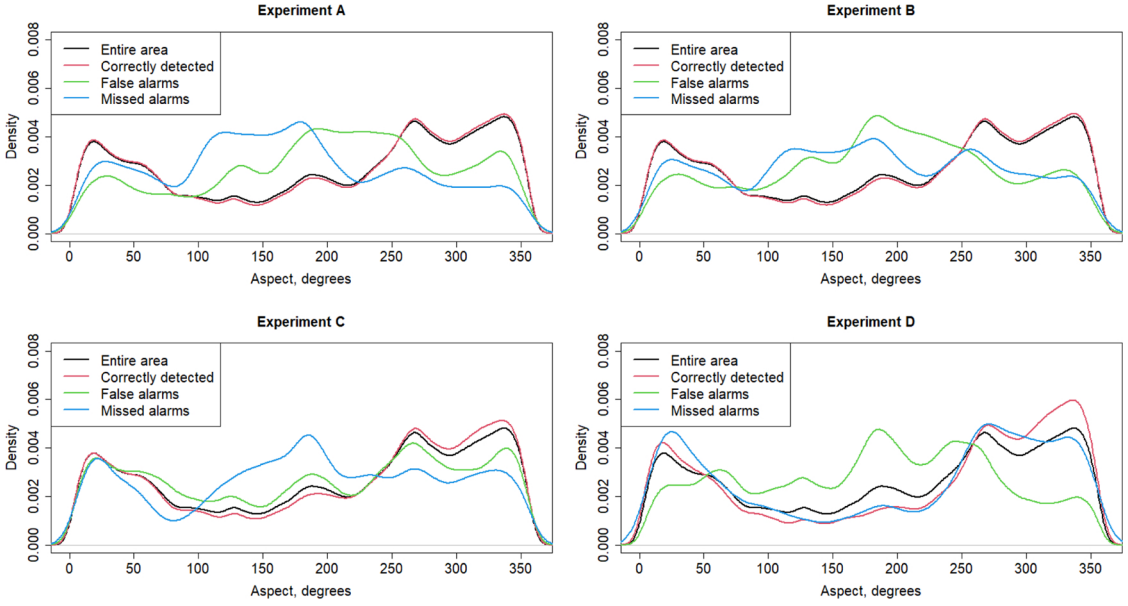

Fig. 6. Density distribution of the aspect for the four experiments in the area where the Manual reference map was drown. The density distribution was computed considering the entire area (black line), only the areas correctly identified as windthrows and non-windthrows (red line), only the areas of false alarms (green line), and only the areas of missed alarms (blue line). (For interpretation of the references to colour in this figure legend, the reader is referred to the web version of this article).

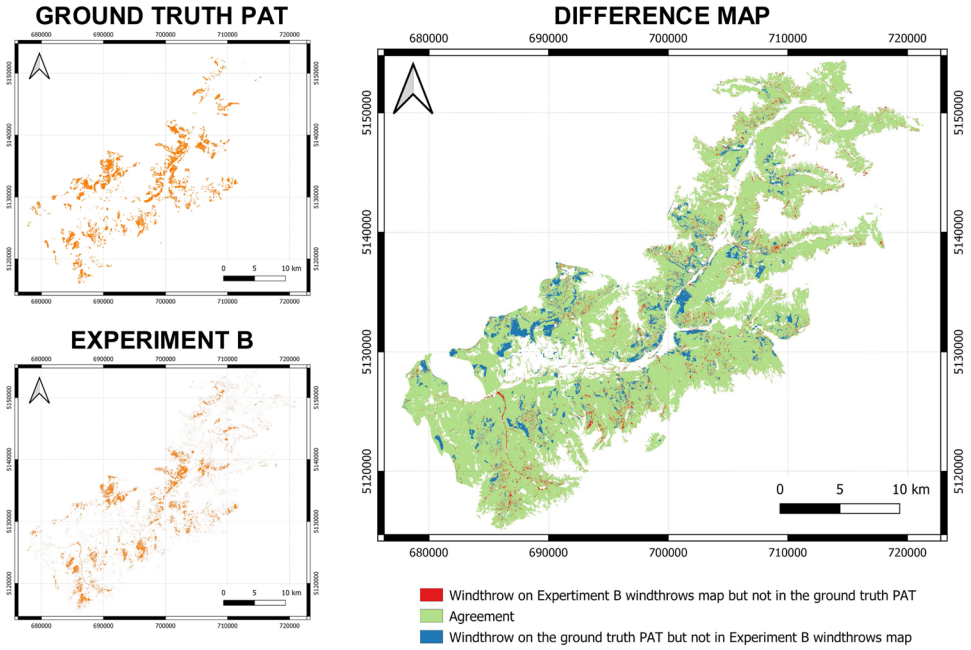

Fig. 7. Windthrow maps over the entire area: i) ground truth PAT map; ii) map obtained in experiment B, and iii) difference map between the previous two.

spatial resolution is the better delineation of the border of the windthrows and the detection of the small windthrow patches. Indeed, false windthrows detection may occur along roads and bare areas at the forest edge, where different vegetation and soil conditions are mixed (Liu et al., 2006), and thus a higher spatial resolution could reduce such problems. Looking at the manual reference map, we can see that the average size of the windthrows areas is 3996 m^2, thus they are also visible in the S2 images that have a pixel size area of 100 m^2. About 25 % of the windthrow areas size of the manual reference map is smaller than the size of the S2 pixels making them hardly traceable in the S2 images. To support this statement, we considered in experiments A and B only windthrows areas of size smaller than the median value of the windthrows patches (288 m^2) and the producer's accuracy of the windthrows moved from a 22.7 % using S2 (experiment A) to a 38.6 % using PS (experiment B). Differently considering only the large areas (above the median value) the producer's accuracy of the windthrows were quite similar for both S2 and PS (81.6 % and 83.5 % respectively). Moreover, if we look at the size of the non-windthrow areas inside large windthrow areas, about 35 % of them are smaller than 100 m^2 thus making them again hardly traceable in S2 images. Looking at the small windthrow areas, obviously they also represent a very small amount of the total damaged areas (0.3 %), but in any case it is useful and important to have them mapped since they are linked to secondary disturbances such as the outbreaks of saproxylic insect species (Bouget and Duelli, 2004). In general, the amount of false alarms is higher than the missed alarms, and this is important as the main interest of the practitioners is to know where the windthrows are and to not miss them in order to avoid insect outbreaks in the long term.

The temporal resolution plays an important role in the probability to obtain an image as soon as possible after a windthrow event. In the specific case analysed in this study, the first available image with S2 was 45 days after the storm, while PS had a good image already after 14 days. Thus, in the case where there is the need to plan the first interventions and to define where to send the field crews to clean up mountain roads, etc. it is very important to have a map as soon as possible, and thus a daily product like PS can outperform S2. There are also other alternatives that could include the use of active sensors (SAR data), that are less influenced by the weather conditions but they require much more complex analysis and they were not considered in this study.

With images acquired in similar conditions (similar phenological status, similar illumination conditions) the results are very good and the windthrows can be mapped with an accuracy above 80 %. Differently, using data acquired near the event the results are not that good, and there is a difference between S2 and PS. It is worth noting that in this case the results obtained are limited to the fact that the analysed windstorm happened in autumn/winter, as probably different conclusions could have been drawn if the event was happening in summertime. In any case, if we look at our specific event, it happened during the transition period between autumn and winter. Autumn 2018 was quite mild in Northern Italy thus many deciduous trees still had leaves/needles on. The storm removed all the leaves/needles from the deciduous species creating areas of change due to this phenomenon. Moreover, suddenly after the storm there was a drop in temperatures and many areas were covered by snow. Also, in open forests, the understory brown off might have played a role in the spectral response and amplified the canopy phenology change. This means that the forest canopies observed in the images acquired in September/October were pretty different from the canopies observed in images acquired in November/December. Additionally, the shadows created by the mountains increased quite a lot, decreasing the sun angle moving from September to December. The different shadows position created another type of changes, and made windthrows happened in North facing slopes hardly detectable. Differently the use of data acquired in June, thus with similar acquisition conditions, minimum shadows due to the sun position, and equal phenological status between deciduous and evergreen trees, maximized the detection rate.

Another important aspect to be considered is the cleaning of the windthrown areas (harvesting operations) through the removal of the tilted/damaged trees, and the presence of regeneration (seedlings). As reported by the forest service of PAT, the challenging environmental/meteorological conditions after the storm have hampered the field operations aiming at the removal of the material (presence of snow and steep slopes). By the end of June 2019, only 26 % of the overall windthrown material in the study area had been collected (Servizio Foreste e Fauna - Provincia Autonoma di Trento, 2020). Therefore, the presence of lying trees might have concurred to the loss of accuracy for the analysis of the winter images, enhancing that of the summer period instead. Moreover, the plantation of seedlings or the presence of natural regeneration in the windthrown areas might lead to errors in the

analysis of images collected in the summer period. In this case, the Forest Service started the plantation of larch seedlings in the period August-September 2019, therefore our analysis might include errors related to the natural regeneration only (Servizio Foreste e Fauna - Provincia Autonoma di Trento, 2020).

When only areas classified as forests of Norway spruce and silver fir were considered, and all the deciduous species were not present, the detection accuracy improved using the near event data. We chose Norway spruce and silver fir as these are the species that were mainly affected by the windthrows event as they are the main species in such areas and also in general the ones more prone to be windthrown (Albrecht et al., 2012; Schmidt et al., 2010). As expected, the improvement is mainly in the false alarms as in experiment C they reduced by about 105 ha, and in experiment D by about 92 ha. These results show us that there is an effect of the species composition in the results obtained in the near event data, especially when the event is in the transition phase between leaves on and off seasons, even in an area like this one where the deciduous species cover a few hectares. We can expect that in the presence of a more mixed forest the effect could be even higher. In that case, if the ecosystem is characterized by only (or mainly) deciduous species, a reasonable solution would be to use additional spectral bands, if available, or to extract additional features. In any case the false alarms are expected to be quite high (if the event has happened near the autumn/winter period) as the problems related to shadows, snow areas and presence of lying trees cannot be removed.

As we stated in the introduction, the vast majority of the previous studies on windthrows used other techniques than CVA (Baumann et al., 2014; Chirici et al., 2019; Duan et al., 2017; Einzmann et al., 2017; Hamdi et al., 2019; Jonikavičius and Mozgeris, 2013; Nyström et al., 2014; Pirotti, 2011; Rich et al., 2010; Rüetschi et al., 2019; Schwarz et al., 2003; Tanase et al., 2018; Vorovencii, 2014; Wang and Xu, 2010). Such techniques rely a lot on a priori knowledge from the user's side on bands combination or spectral indices to be used. Whereas CVA in the polar domain takes advantage of the statistical distribution of the pixels in the difference image (X_D) in order to further understand the behaviour of the data. Yet, the problem of automatically finding these thresholds remains not only for CVA, but also for all the other methods in literature.

Considering previous studies using satellite remote sensing data to map windthrows, our results are similar or better in terms of accuracies. In Baumann et al. (2014) a disturbance index computed using Landsat data was used to map windthrows in a mixed forest of Norway spruce and Scots pine. The authors validated the results on a manually delineated reference map obtaining a kappa accuracy around 0.55 and an overall accuracy around 77 %. Einzmann et al. (2017) used Random Forest and object based change detection techniques on RapidEye data in a Norway spruce forest. The validation was done on both a manually delineated map and on forest inventory data and they obtained an overall accuracy of 93 %. Jonikavičius and Mozgeris (2013) used image difference of Landsat bands and k-Nearest Neighbour with manual thresholding and they obtained overall accuracies between 95–98 %. In Schwarz et al. (2003) four data sources were considered (i.e. Landsat 7, Spot 4, IKONOS and SAR) together with classification methods and the authors obtained kappa accuracies between 0.46 and 0.51. In the study of Wang and Xu (2010), CVA was compared with other techniques using different types of features extracted from Landsat data. The results changed according to the features used and the kappa ranged from 0.02 to 0.72. Other studies exist that used airborne or UAV data. In such cases results are maybe better (mainly due to the highest spatial resolution) but obviously the costs for the data acquisitions were much higher compared to satellite data, especially compared to S2 data that are freely available.

Regarding the threshold's selection, if the goal is to get a binary CD map only (change and no change), applying a threshold over the magnitude variable is enough (Bovolo and Bruzzone, 2007). A different scenario has to be considered when the problem to be analysed implies the identification of different types of changes, or a specific type of change, as it is our case, where windthrows have to be separated from any other types of change. In fact, we exploited the CVA in the polar domain, where different kinds of changes tend to fall in the same sector (see Fig. 3). Because of this, it is expected to have different thresholds for the magnitude variable along different datasets, but slightly similar ones for the direction variable (see Table 4). This characteristic allowed us to obtain the different thresholds in a relatively easy way, resulting in a high detection accuracy. However, if different types of changes with similar nature occur at the same time, i.e., several types of changes due to different types of vegetation in the area, the selection of these thresholds becomes harder, leading to a reduction in the final accuracy detection. This was observed for experiments C and D, where more than one change was present (i.e. windthrows, illumination conditions, and phenological phase). Additionally, shaded areas due to the irradiation angle and the mountainous landscapes can also hamper the recognition of important changes, altering the CVA performance.

6. Conclusions

In this study we showed that both S2 and PS data are suitable to detect windthrows with high levels of accuracy (OA above 90 % and PA of windthrows class above 80 %). Furthermore, we also showed the suitability of CVA for detecting windthrows independently of the multispectral images and the weather conditions. The data considered are characterized by very different resolutions (spectral, spatial, and temporal) but the results obtained in both scenarios are very similar. With both data it emerged that the infrared bands are very important to obtain high accuracies, in particular it is necessary to combine a band in the visible spectral range with one in the infrared. The acquisition conditions strongly affect the accuracy in detecting windthrows, though it depends on the season in which the windthrows happened and on the topography of the area. In the case of windthrows happening in fall season, it was clear that data acquired in non-optimal conditions do not allow to have a proper detection of the windthrows, reducing the final accuracy.

CRediT authorship contribution statement

Michele Dalponte: Conceptualization, Methodology, Software, Formal analysis, Writing - original draft, Writing - review & editing. **Sebastian Marzini:** Conceptualization, Methodology, Software, Formal analysis, Writing - original draft, Writing - review & editing. **Yady Tatiana Solano-Correa:** Conceptualization, Methodology, Software, Formal analysis, Writing - original draft, Writing - review & editing. **Giustino Tonon:** Conceptualization, Writing - review & editing, Project administration. **Loris Vescovo:** Conceptualization, Methodology, Writing - original draft, Writing - review & editing. **Damiano Gianelle:** Conceptualization, Writing - review & editing, Project administration.

Declaration of Competing Interest

The authors declare that they have no known competing financial interests or personal relationships that could have appeared to influence the work reported in this paper.

Acknowledgement

The authors would like to thank Planet Labs Inc. for providing the images used in this study under the "Education and Research program". This work was patially funded by the Highlander project co-financed by the Connecting European Facilty Programme of the European Union Grant agreement n° INEA/CEF/ICT/A2018/1815462.

Appendix A. Supplementary data

Supplementary material related to this article can be found, in the online version, at doi:https://doi.org/10.1016/j.jag.2020.102206.

References

Albrecht, A., Hanewinkel, M., Bauhus, J., Kohnle, U., 2012. How does silviculture affect storm damage in forests of south-western Germany? Results from empirical modeling based on long-term observations. Eur J Forest Res 131, 229–247. https://doi.org/10.1007/s10342-010-0432-x.

Baumann, M., Ozdogan, M., Wolter, P.T., Krylov, A., Vladimirova, N., Radeloff, V.C., 2014. Landsat remote sensing of forest windfall disturbance. Remote Sens. Environ. 143, 171–179. https://doi.org/10.1016/j.rse.2013.12.020.

Cat Berro, D., Acordon, V., Castellano, C., 2018. 27-30 Ottobre 2018: Scirocco Eccezionale, Mareggiate E Alluvioni in Italia Con La Tempesta “Vaia”. [WWW Document]. URL http://www.nimbus.it/eventi/2018/181031TempestaVaia.htm (accessed 4.6.20). .

Bouget, C., Duelli, P., 2004. The effects of windthrow on forest insect communities: a literature review. Biol. Conserv. 118, 281–299. https://doi.org/10.1016/j.biocon.2003.09.009.

Bovolo, F., Bruzzone, L., 2007. A theoretical framework for unsupervised change detection based on change vector analysis in the polar domain. Ieee Trans. Geosci. Remote. Sens. 45, 218–236. https://doi.org/10.1109/TGRS.2006.885408.

Bovolo, F., Bruzzone, L., Solano-Correa, Y.T., 2018. Multitemporal analysis of remotely sensed image data. In: Liang, S. (Ed.), Comprehensive Remote Sensing. Elsevier, Oxford, pp. 156–185. https://doi.org/10.1016/B978-0-12-409548-9.10338-0.

Ceccato, P., Flasse, S., Tarantola, S., Jacquemoud, S., Grégoire, J.-M., 2001. Detecting vegetation leaf water content using reflectance in the optical domain. Remote Sens. Environ. 77, 22–33. https://doi.org/10.1016/S0034-4257(01)00191-2.

Ceccato, P., Gobron, N., Flasse, S., Pinty, B., Tarantola, S., 2002. Designing a spectral index to estimate vegetation water content from remote sensing data: part 1. Remote Sens. Environ. 82, 188–197. https://doi.org/10.1016/S0034-4257(02)00037-8.

Chirici, G., Giannetti, F., Travaglini, D., Nocentini, S., Francini, S., D’Amico, G., et al., 2019. Forest Damage Inventory After the “Vaia” Storm in Italy. Forest@ - Rivista Di Selvicoltura Ed Ecologia Forestale 16. pp. 3–9. https://doi.org/10.3832/efor3070-016.

Duan, F., Wan, Y., Deng, L., 2017. A novel approach for coarse-to-Fine windthrown tree extraction based on unmanned aerial vehicle images. Remote Sens. (Basel) 9, 306. https://doi.org/10.3390/rs9040306.

Einzmann, K., Immitzer, M., Böck, S., Bauer, O., Schmitt, A., Atzberger, C., 2017. Windthrow detection in european forests with very high-resolution optical data. Forests 8, 21. https://doi.org/10.3390/f8010021.

Haidu, I., Furtuna, P.R., Lebaut, S., 2019. Detection of old scattered windthrow using low cost resources. The case of Storm Xynthia in the Vosges Mountains, 28 February 2010. Open Geosci. 11, 492–504. https://doi.org/10.1515/geo-2019-0040.

Hamdi, Z.M., Brandmeier, M., Straub, C., 2019. Forest damage assessment using deep learning on high resolution remote sensing data. Remote Sens. (Basel) 11, 1976. https://doi.org/10.3390/rs11171976.

Houborg, R., McCabe, M.F., 2018. A Cubesat enabled spatio-temporal enhancement method (CESTEM) utilizing planet, landsat and MODIS data. Remote Sens. Environ. 209, 211–226. https://doi.org/10.1016/j.rse.2018.02.067.

Jalkanen, A., Mattila, U., 2000. Logistic regression models for wind and snow damage in northern Finland based on the National Forest Inventory data. For. Ecol. Manage. 135, 315–330. https://doi.org/10.1016/S0378-1127(00)00289-9.

Johnson, R.D., Kasischke, E.S., 1998. Change vector analysis: a technique for the multispectral monitoring of land cover and condition. Int. J. Remote Sens. 19, 411–426. https://doi.org/10.1080/014311698216062.

Jonikavičius, D., Mozgeris, G., 2013. Rapid assessment of wind storm-caused forest damage using satellite images and stand-wise forest inventory data. iForest Biogeosci. For. 6, 150. https://doi.org/10.3832/ifor0715-006.

Liu, D., Kelly, M., Gong, P., 2006. A spatial–temporal approach to monitoring forest disease spread using multi-temporal high spatial resolution imagery. Remote Sens. Environ. 101, 167–180. https://doi.org/10.1016/j.rse.2005.12.012.

Mitchell, S.J., 2013. Wind as a natural disturbance agent in forests: a synthesis. Forestry Lond. (Lond) 86, 147–157. https://doi.org/10.1093/forestry/cps058.

Moreau, S., Bosseno, R., Gu, X.F., Baret, F., 2003. Assessing the biomass dynamics of Andean bofedal and totora high-protein wetland grasses from NOAA/AVHRR. Remote Sens. Environ. 85, 516–529. https://doi.org/10.1016/S0034-4257(03)00053-1.

Nyström, M., Holmgren, J., Fransson, J.E.S., Olsson, H., 2014. Detection of windthrown trees using airborne laser scanning. Int. J. Appl. Earth Obs. Geoinf. 30, 21–29. https://doi.org/10.1016/j.jag.2014.01.012.

Pirotti, F., 2011. Analysis of full-waveform LiDAR data for forestry applications: a review of investigations and methods. iForest Biogeosci. For. 4, 100–106. https://doi.org/10.3832/ifor0562-004.

PlanetTeam, 2017. Planet Application Program Interface: In Space for Life on Earth. San Fracisco, CA. .

QGIS Development Team, 2020. QGIS Geographic Information System. Open Source Geospatial Foundation Project [WWW Document]. URL. https://qgis.org/it/site/.

R Core Team, 2017. R: a Language and Environment for Statistical Computing. Vienna, Austria. https://doi.org/ISBN3-900051-07-0. .

Rich, RoyL., Frelich, L., Reich, P.B., Bauer, M.E., 2010. Detecting wind disturbance severity and canopy heterogeneity in boreal forest by coupling high-spatial resolution satellite imagery and field data. Remote Sens. Environ. 114, 299–308. https://doi.org/10.1016/j.rse.2009.09.005.

Roemer, H., Kaiser, G., Sterr, H., Ludwig, R., 2010. Using remote sensing to assess tsunami-induced impacts on coastal forest ecosystems at the Andaman Sea coast of Thailand. Nat. Hazards Earth Syst. Sci. 10, 729–745. https://doi.org/10.5194/nhess-10-729-2010.

Ruel, J.-C., 1995. Understanding windthrow: silvicultural implications. For. Chron. 71, 434–445. https://doi.org/10.5558/tfc71434-4.

Rüetschi, M., Small, D., Waser, L.T., 2019. Rapid detection of windthrows using Sentinel-1 C-Band SAR data. Remote Sens. (Basel) 11, 115. https://doi.org/10.3390/rs11020115.

Schelhaas, M.-J., 2008. Impacts of natural disturbances on the development of European forest resources: application of model approaches from tree and stand levels to large-scale scenarios. Diss. For. 2008. https://doi.org/10.14214/df.56.

Schmidt, M., Hanewinkel, M., Kändler, G., Kublin, E., Kohnle, U., 2010. An inventory-based approach for modeling single-tree storm damage — experiences with the winter storm of 1999 in southwestern Germany. Can. J. For. Res. 40, 1636–1652. https://doi.org/10.1139/X10-099.

Schwarz, M., Steinmeier, C., Holecz, F., Stebler, O., Wagner, H., 2003. Detection of Windthrow in Mountainous Regions with Different Remote Sensing Data and Classification Methods. Scand. J. For. Res. 18, 525–536. https://doi.org/10.1080/02827580310018023.

Seidl, R., Schelhaas, M.-J., Rammer, W., Verkerk, P.J., 2014. Increasing forest disturbances in Europe and their impact on carbon storage. Nat. Clim. Chang. 4, 806–810. https://doi.org/10.1038/nclimate2318.

Servizio Foreste e Fauna - Provincia Autonoma di Trento, 2018. Stato d’attuazione Del Piano d’azione Per La Gestione Degli Interventi Di Esbosco E Ricostruzione Dei Boschi Danneggiati Dagli Eventi Eccezionali Nei Giorni Dal 27 Al 30 Ottobre 2018 - 1° Report 2018. Trento, Italy. .

Servizio Foreste e Fauna - Provincia Autonoma di Trento, 2020. Stato d’attuazione Del Piano d’azione Per La Gestione Degli Interventi Di Esbosco E Ricostruzione Dei Boschi Danneggiati Dagli Eventi Eccezionali Nei Giorni Dal 27 Al 30 Ottobre 2018-2° Report 2019. Trento, Italy. .

Singh, S., Talwar, R., 2014. A comparative study on change vector analysis based change detection techniques. Sadhana 39, 1311–1331. https://doi.org/10.1007/s12046-014-0286-x.

Solano-Correa, Y.T., Bovolo, F., Bruzzone, L., 2014. Change Detection in Very High Resolution Multisensor Optical Images. pp. 924410-924410–13.. https://doi.org/10.1117/12.2068171.

Solano-Correa, Y.T., Bovolo, F., Bruzzone, L., 2016. An approach to multiple change detection in multisensor VHR optical images based on iterative clustering. 2016 IEEE International Geoscience and Remote Sensing Symposium (IGARSS). Presented at the 2016 IEEE International Geoscience and Remote Sensing Symposium (IGARSS) 5149–5152. https://doi.org/10.1109/IGARSS.2016.7730342.

Solano-Correa, Y.T., Bovolo, F., Bruzzone, L., 2019a. Generation of homogeneous VHR time series by nonparametric regression of multisensor bitemporal images. Ieee Trans. Geosci. Remote. Sens. 57, 7579–7593. https://doi.org/10.1109/TGRS.2019.2914397.

Solano-Correa, Y.T., Bovolo, F., Bruzzone, L., 2019b. An approach to multiple change detection in VHR optical images based on iterative clustering and adaptive thresholding. Ieee Geosci. Remote. Sens. Lett. 16, 1334–1338. https://doi.org/10.1109/LGRS.2019.2896385.

Tanase, M.A., Aponte, C., Mermoz, S., Bouvet, A., Le Toan, T., Heurich, M., 2018. Detection of windthrows and insect outbreaks by L-band SAR: a case study in the Bavarian Forest National Park. Remote Sens. Environ. 209, 700–711. https://doi.org/10.1016/j.rse.2018.03.009.

Thiagarajan, A., MacDonald, M.T., Lada, R., 2016. Environmental and hormonal physiology of postharvest needle abscission in christmas trees. Crit. Rev. Plant Sci. 35, 1–17. https://doi.org/10.1080/07352689.2015.1133965.

Vilhar, U., Beuker, E., Mizunuma, T., Skudnik, M., Lebourgeois, F., Soudani, K., Wilkinson, M., 2013. Tree phenology, Forest monitoring. Terrestrial Methods in Europe With Outlook to Norht America and Asia. pp. 169–182. https://doi.org/10.1016/B978-0-08-098222-9.00009-1. Amsterdam, The Netherlands.

Vogelmann, J.E., 1990. Comparison between two vegetation indices for measuring different types of forest damage in the north-eastern United States. Int. J. Remote Sens. 11, 2281–2297. https://doi.org/10.1080/01431169008955175.

Vorovencii, I., 2014. Detection of environmental changes due to windthrows using landsat 7 etm+ satellite images. Environ. Eng. Manage. J. 13, 565–576.

Wang, F., Xu, Y.J., 2010. Comparison of remote sensing change detection techniques for assessing hurricane damage to forests. Environ. Monit. Assess. 162, 311–326. https://doi.org/10.1007/s10661-009-0798-8.

Xue, J., Su, B., 2017. Significant remote sensing vegetation indices: a review of developments and applications. J. Sens. 2017, 1–17. https://doi.org/10.1155/2017/1353691.

Yong, Du, Cihlar, J., Beaubien, J., Latifovic, R., 2001. Radiometric normalization, compositing, and quality control for satellite high resolution image mosaics over large areas. Ieee Trans. Geosci. Remote. Sens. 39, 623–634. https://doi.org/10.1109/36.911119.

Yuan, D., Elvidge, C.D., 1996. Comparison of relative radiometric normalization techniques. Isprs J. Photogramm. Remote. Sens. 51, 117–126. https://doi.org/10.1016/0924-2716(96)00018-4.

Zanetti, M., Bovolo, F., Bruzzone, L., 2015. Rayleigh-rice mixture parameter estimation via EM algorithm for change detection in multispectral images. Ieee Trans. Image Process. 24, 5004–5016. https://doi.org/10.1109/TIP.2015.2474710.